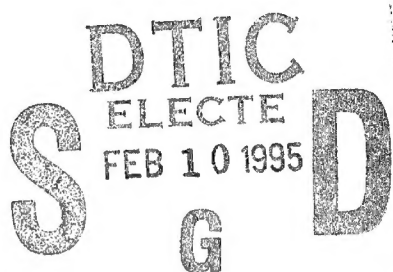UIME PBB 94-003

A Thermochemical Transport Model for Analysis of Hot-Spot Formation in Energetic Materials

Final Report
ARO Contract: DAAL03-91-G-0020

P.B. Butler and D. Bonnett
Department of Mechanical Engineering

2 December, 1994

DTIC
ELECTE
FEB 1 0 1995
S
G
D

19950203 242

THE UNIVERSITY OF IOWA

Iowa City, Iowa 52242

REPORT DOCUMENTATION PAGE		Form Approved OMB No. 0704-0188

Public reporting burden for this collection of information is estimated to average 1 hour per response, including the time for reviewing instructions, searching existing data sources, gathering and maintaining the data needed, and completing and reviewing the collection of information. Send comments regarding this burden estimate or any other aspect of this collection of information, including suggestions for reducing this burden, to Washington Headquarters Services, Directorate for Information Operations and Reports, 1215 Jefferson Davis Highway, Suite 1204, Arlington, VA 22202-4302, and to the Office of Management and Budget, Paperwork Reduction Project (0704-0188), Washington, DC 20503.

1. AGENCY USE ONLY (Leave blank)	2. REPORT DATE 2 Dec 1994	3. REPORT TYPE AND DATES COVERED Final Report; 1 Jan 1991 – 31 Aug 1994

4. TITLE AND SUBTITLE	5. FUNDING NUMBERS
A Thermochemical Transport Model for Analysis of Hot-Spot Formation in Energetic Materials	
6. AUTHOR(S) P. Barry Butler and David Bonnett	$DAAL03-91-G-0020$

7. PERFORMING ORGANIZATION NAME(S) AND ADDRESS(ES) The University of Iowa Department of Mechanical Engineering Iowa City, IA 52242	8. PERFORMING ORGANIZATION REPORT NUMBER UIME PBB-94-003

9. SPONSORING/MONITORING AGENCY NAME(S) AND ADDRESS(ES) U.S. Army Research Office P.O. Box 12211 Research Triangle Park, NC 27709-2211	10. SPONSORING/MONITORING AGENCY REPORT NUMBER $ARO\ 28310.3-EG$

11. SUPPLEMENTARY NOTES
The views, opinions and/or findings contained in this report are those of the author(s) and should not be construed as an official Department of the Army position, policy, or decision, unless so designated by other documentation.

12a. DISTRIBUTION/AVAILABILITY STATEMENT Approved for public release; distribution unlimited.	12b. DISTRIBUTION CODE

13. ABSTRACT (Maximum 200 words)

The focus of this research is on the prediction of inadvertent ignition and detonation of condensed-phase, energetic materials. Specifically, the work focuses on hot spot formation in high-energy propellants and explosives. A viscoplastic pore collapse model is developed to analyze the potential for hot spot formation in porous, condensed-phase, energetic materials. This model treats the dynamics and thermodynamics of a collapsing spherical void that has been subjected to weak shock loading. An volume-averaged energy balance is used to track temporal variations of the pore gas temperature, and a finite-difference method is used to solve the complete condensed-phase energy equation in the vicinity of a material discontinuity. Results from sample calculations focus on the interfacial energy balance in predicting the rate of localized temperature increase during shock compression.

14. SUBJECT TERMS Hot-Spots, Ignition, Shock Heating, Energetic Materials			15. NUMBER OF PAGES 37
			16. PRICE CODE

17. SECURITY CLASSIFICATION OF REPORT UNCLASSIFIED	18. SECURITY CLASSIFICATION OF THIS PAGE UNCLASSIFIED	19. SECURITY CLASSIFICATION OF ABSTRACT UNCLASSIFIED	20. LIMITATION OF ABSTRACT UL

A Thermochemical Transport Model for Analysis of Hot-Spot Formation in Energetic Materials

Final Report
(Report Number: UIME PBB-94-003)

P. B. Butler and David Bonnett
Department of Mechanical Engineering
The University of Iowa
Iowa City, Iowa 52242

2 December, 1994

Accesion For		
NTIS CRA&I		☒
DTIC TAB		☐
Unannounced		☐
Justification		
By		
Distribution /		
Availability Codes		
Dist	Avail and / or Special	
A-1		

APPROVED FOR PUBLIC RELEASE;
DISTRIBUTION UNLIMITED

TABLE OF CONTENTS

1 INTRODUCTION

1.1 Motivation

During the development stage of condensed-phase, energetic materials (propellants and explosives) there is often a trade-off between performance, associated with energy content of the material, and the potential for inadvertent ignition and transition to detonation [1,2]. In the case of rocket propellants, thrust and specific impulse are often improved by the addition of high-energy ingredients (i.e., RDX and HMX) to the propellant formulation [3]. It is well documented that initiation scenarios are possible during all phases of the energetic material's life cycle including; processing, transportation, testing, handling, and use [4]. The interest in developing energetic materials that are both high performance and insensitive has led to a significant quantity of research focused primarily on characterizing the sensitivity of energetic materials to various stimuli (thermal, mechanical, and electrical), and on identifying the mechanisms involved in initiation and detonation. Development of methods to predict the hazards associated with current energetic materials, and the incorporation of these methods into the design process for new formulations, is the ultimate goal of much of the previous research [5].

Unfortunately, an understanding of energetic material initiation mechanisms at a fundamental level is a difficult task. Many of the current test methods are considered inadequate for hazards characterization since they provide little insight into the actual physical processes occurring during an initiation event [2]. Until the recent development of advanced experimental techniques, most of the previous studies were limited to examining the effects of material parameters, such as porosity, on initiation sensitivity, and on characterizing the initiation properties of specific energetic materials subjected to different stimuli [6]. These tests are often expensive, the results are difficult to relate to practical scenarios, and the knowledge gained can only be incorporated into the design process after the fact [2]. In addition, many of the current modeling efforts, such as shock initiation hydrocodes (codes which model the dynamics of stress wave propagation through a material), rely on oversimplified and often unrealistic assumptions of chemical kinetic processes to model energy release in the material. Many of the current hydrocodes rely on empirical curve fits to reconcile model predictions with experiments [2]. Due to the predictive shortcomings in both modeling and experiments, it is highly desirable to develop a model based on first principles that can provide an understanding of the fundamental physical processes that occur during the initiation of an energetic material.

The research discussed here is based on a micromechanics approach to hot spot formation and growth to detonation [7]. Hot spot thermal histories predicted by this model are the direct result of solving basic conservation laws (mass, momentum, energy) for a small control volume of material adjacent to an internal void that has been shock compressed. While microscopic hot spot models

1

such as this predict the history of a single hot spot, it should be emphasized they do not relate directly to experimentally measured quantities such as detonation run-up distance. That is, the formation and evolution of a single hot spot cannot uniquely determine the response of the bulk material during shock impact. The two are closely coupled through the fundamental hydrodynamic and thermodynamic attributes of the material, processes that are beyond the scope of the present work.

1.2 Background

Previous research has shown that a small fraction of voids in a condensed-phase, energetic material can substantially increase the materials sensitivity to initiation by shock impact [5-8]. This ignition phenomenon is clearly demonstrated when certain high-energy propellant formulations and explosives are observed to detonate at shock pressures well below the level necessary for thermal ignition from bulk heating alone. In some cases, the energy transmitted from a relatively weak shock wave is sufficient to initiate a sustained reaction which, following an induction period, can transition to a high-order detonation. Although the exact physical processes which occur during ignition are unknown, it is generally accepted that initiation in the energetic material begins at isolated 'hot spots' in the material. The hot spots are formed when mechanical or electrical energy from an external stimulus is converted into heat at highly localized regions, usually at or near discontinuities in the material. Hot spot initiation occurs at locations that retain sufficient thermal energy to start chemical reactions in the material. This phenomenon was very clearly demonstrated in the recent work of Baillou [8], where several batches of nearly identical RDX crystals showed significantly different shock ignition thresholds. It was noted that the only difference between the two samples was the size and quantity of internal voids due to their respective manufacturing processes.

Several thermo-mechanical mechanisms have been suggested [9-13] as potential hot spot sources. These include: friction between adjacent grains, jetting of material fragments across voids, hydrodynamic pore collapse, viscous heating and internal shear, and shock interactions at density discontinuities. Much of the experimental data and analytical modeling of hot spots indicate that the specific mechanisms responsible for hot spot formation depend on the physical and thermodynamic properties of the heterogeneous materials, as well as the means by which the energy is transmitted to the material from an external source (e.g., shock, shear, thermal heating, fragment impact, etc.). For low porosity (< 10%) shock-impacted nitramines, Khasainov et al. [9] postulate that heating due to plastic work at pore interfaces is the dominant mechanism for hot spot ignition. Others that have contributed to the understanding of viscoplastic heating effects in energetic materials include: Butcher, Carrol, and Holt [14], Khasainov, Borisov, and Ermolayev [15], Dunin and Surkov [16], Attetkov, Vlasova, Selivanov, and Solov'ev [17], and Maiden [18].

2

1.3 Hot Spot Mechanism

Two key elements in understanding the detonation hazard associated with energetic materials include the identification of the dominant physical processes involved in: 1) hot spot formation, and 2) the subsequent growth to detonation or quenching of the reaction. Research suggests that hot spot formation depends strongly on the microstructural, mechanical, thermal, and chemical properties of the material. It is important, therefore, for any predictive model to include these affects. Item 1, hot spot formation, is the focus of the research reported here. The work focuses on the thermal/mechanical processes that act to transfer compression work of the shock wave into localized high-temperature ignition sites. It is shown that under certain initial conditions (pore size, shock pressure, etc.), localized heating can lead to release of chemical energy that exceeds that dissipated by heat losses. Under these conditions the reaction and hot spot can grow, coalesce with other hot spots and start large scale deflagration (burning) of the bulk material, which can lead to detonation.

An illustration of the process of hot spot initiation by shock wave, leading to detonation, is shown in Fig. 1.1 [20]. This figure shows a snapshot in time when the material behind the shock is at various stages of decomposition. In order to model the complete sequence of events associated with inadvertent ignition leading to detonation, one must couple the transient behavior of each Lagrangian material location with the overall hydrodynamic attributes of the propagating shock wave. The current research focuses on the micromechanical processes that occur in the vicinity of a single void.

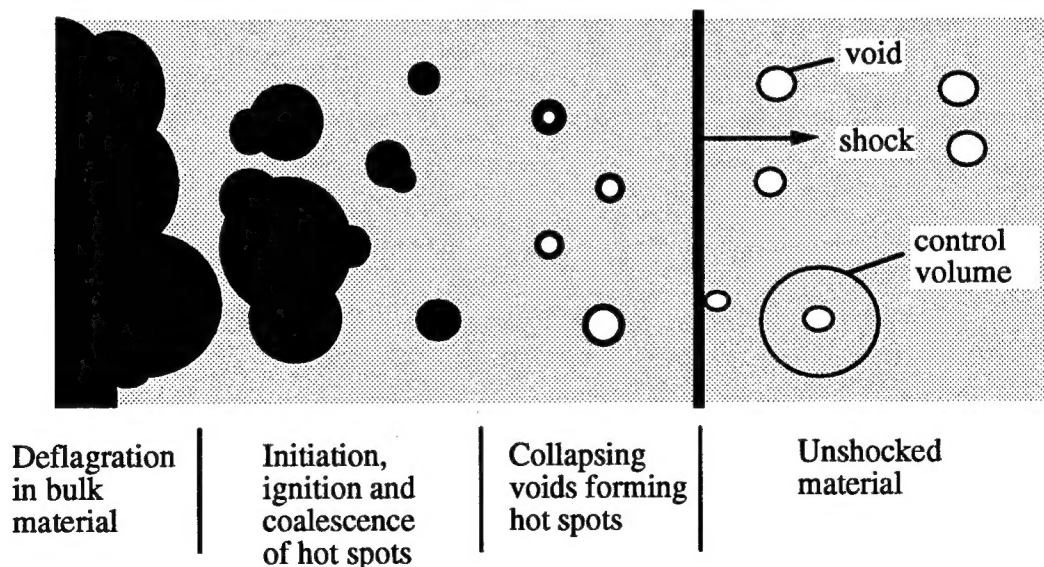| Deflagration in bulk material | Initiation, ignition and coalescence of hot spots | Collapsing voids forming hot spots | Unshocked material |

Fig. 1.1 Illustration of shock induced, hot spot formation and growth, in a porous, condensed-phase, energetic material (The darkened area represents material that has burned). Sketch reproduced from [20].

3

1.4 Research Objectives

The main goal of this research is to develop methods to minimize the possibility of inadvertent ignition and detonation of energetic materials. It is virtually impossible to design less shock sensitive energetic materials without a knowledge of the physical processes occurring during hot spot ignition. Important physical processes involved in hot spot formation are known to include; heating effects due to the interaction of the shock wave with a void in an energetic material, melting of the energetic material, heat conduction in the material, and chemical reaction in the material. Of special interest in this research is the determination of the dominant physical processes occurring at different times during hot spot formation. In addition, it is known that hot spot formation is highly dependent on the mechanical, thermal, and chemical properties of the energetic material. The role that some of these properties play in hot spot formation is examined.

To analyze the mechanisms involved in hot spot formation in porous, condensed-phase, energetic materials a micromechanical model, based the conservation equations, has been developed. This model treats the dynamics and thermodynamics of a collapsing spherical void and the energetic material surrounding the void that have been subjected to a known stress-time profile. Processes such as viscoplastic heating, phase change, finite-rate chemical reactions, heat and mass transfer between the condensed phase and the void are included in the model. Heat conduction in the condensed phase is modeled using a finite difference method. A gas-phase energy balance is used to track gas-phase temperature. Temperature and pressure dependent viscosity, yield strength, and melt temperature, in the condensed phase are included. The sample results presented here treat a nonreactive material with constant physical properties. For additional results including reactivity and temperature-dependent material properties, see [7].

4

2 REVIEW OF LITERATURE

2.1 Introduction

As mentioned in the previous section, shock ignition of heterogeneous, energetic materials has been studied a great deal in recent years. Advances in experimental and modeling techniques have led to significant progress in understanding the thermo-physical processes of shock initiation. It is generally agreed that initiation begins from very small hot spots, created by highly localized heating in the material. This section presents a brief overview of some of the most widely proposed models for hot spot formation including; adiabatic compression of trapped gas, localized adiabatic shear of the material during mechanical failure, hydrodynamic shock focusing, and viscoplastic void collapse.

2.2 Non-Viscoplastic Hot Spot Mechanisms

A general consensus has emerged from much of the research conducted in the area of shock initiation of heterogeneous energetic materials. It is generally accepted that; 1) initiation in these materials occurs at isolated, high temperature regions called hot spots, 2) these hot spots are thermal in origin and are usually formed from the interaction of the shock wave with defects in the material, and 3) hot spot formation depends on the material's mechanical, thermal and chemical properties. Contention arises, however, in the many different mechanisms of hot spot generation that have been proposed over the years [21,22].

It is well known that the introduction of voids in energetic materials causes increased sensitivity to shock ignition. In fact, explosive manufacturers commonly add artificial cavities to increase the detonability of insensitive energetic materials [23]. For this reason, many of the proposed hot spot models focus on shock induced void or cavity collapse as the mechanism of hot spot formation. These models include the adiabatic compression of gas in a collapsing cavity, hydrodynamic cavity collapse, viscoplastic heating of the condensed-phase material surrounding a collapsing cavity, and the development of shear bands in the solid.

2.2.1 Adiabatic Gas Compression

Bowden and Yoffee were among the first researchers to show that the rapid compression of gas filled cavities is a key factor in the shock sensitivity of liquid explosives [24]. These researchers suggested that gas trapped in a shock collapsed void is compressed adiabatically to a very high temperature. Energetic material surrounding the void is then heated by the high temperature void gas. Chemical reactions, leading to initiation of the energetic material, may result if the material temperature exceeds the ignition temperature.

Advances in high speed photographic techniques have allowed researchers to directly photograph bubble collapse in shocked materials. Chaudhri and Field [25] photographed air bubbles in water as it was collapsed by weak shock waves ($P_S \sim 1$ GPa). The bubbles studied in this work ranged in size from 50 μm $< d <$ 1 mm. When these collapsed bubbles were placed in contact with a sensitive explosive (AgO_3), initiation was observed. When a collapsing air bubble of the same size was placed only a few micrometers from the explosive surface, no ignition occurred. The gas specific heat, which was expected to play an important role in the transfer of heat from a gas to a solid, was found to be was found to be a critical parameter in the ignition of the explosive.

Field, Swallowe, and Heavens [26] photographed the low velocity collision of two ($d = 0.2$ mm) bubbles in nitroglycerin. After the collision, a slit-shaped air gap trapped between the drops was compressed, and subsequently led to ignition of the nitroglycerin along the entire length of the air gap. It was concluded that the pressure generated by the collision was much too low to cause ignition of homogeneous nitroglycerin, and that ignition was caused by the high temperature in the air gap caused by gas compression.

Conducting experimental and modeling work, Starkenburg [27] concluded that gas compression does not occur adiabatically. However, it was shown that gas compression is a dominant mechanism in hot spot formation if the gas compression rate, compared to that of shock compression, is low, and relatively large void sizes ($d > 1$ mm) are compressed.

It is also known that cavities subjected to stronger shock waves can collapse asymmetrically to produce a liquid jet in the void. This high speed liquid jet then impinges on the downstream side of the cavity, effectively isolating the gas into two lobes. These lobes then collapse compressing the gas trapped inside. Bourne and Field [28] studied large air bubbles ($3 < d < 12$ mm) in inert gelatin, collapsed by shocks of strength $P_s < 3.5$ GPa. These researchers detected light emission from the two compressed gas lobes, and estimated that temperatures from 750 - 1000 K were achieved in the adiabatically compressed gas. Partom [29] used the adiabatic gas compression model, coupled with a one-dimensional hydrodynamic-reactive code, to calculate the entire hot spot formation, and subsequent growth-to-detonation process in the explosive PETN.

These experimental and modeling results show that adiabatic gas compression is, in some cases, a viable mechanism for hot spot formation. However, other experimental work has shown that this mechanism is not the controlling mechanism for most shock initiation situations, which have higher compression rates [30].

2.2.2 Hydrodynamic Void Collapse

Another void collapse model was proposed by Mader [31,32] to explain hot spot formation due to shock wave interaction with density discontinuities. In this model the upstream surface of a

6

cavity in a compressible energetic material is accelerated by a shock wave and impinges on the downstream side of the cavity. This high-speed impact produces a high impact pressure which is amplified by convergence effects during the cavity collapse. The hot spot is caused by heating produced by the compression of the solid-phase material from the high pressure impact. Mader incorporated this model into a two-dimensional numerical hydrodynamics code to compute hot spot formation and detonation in nitromethane.

2.2.3 Localized Adiabatic Shear (Shear Bands)

It is well known that plastic deformation is an efficient way to convert mechanical energy to thermal energy [26]. In most crystalline solids, plastic flow occurs inhomogeneously along crystallographic slip planes, called shear bands. A temperature rise in the deforming material, due to energy dissipation by plastic and viscous work, is likely to be non-uniformly distributed along these shear bands, with the material outside of these bands undergoing little or no plastic deformation and heating. Significant local temperature rises, leading to hot spot formation can occur due to this deformation [33].

Recent advances in experimental methods, including high-speed photography and heat sensitive film techniques, have allowed direct observation of shear bands in explosive crystals subjected to shock and impact [34]. Field, Swallowe, and Heavens [26] and Field, Palmer and Parry, [34] have shown that localized shear appears in samples of explosives impacted at levels just below that required for ignition. These and other researchers have also shown that ignition begins at, and propagates from, clearly visible shear bands during high velocity impact testing.

Grady and Kipp [35] have derived expressions for shear band spacing, width, and growth times based on catastrophic growth model of unstable thermoplastic shear. These calculations relate shear band characteristics with thermal properties of the material and the dynamic loading data. Krishna Mohan, Bhasu, and Field [36] have compared impact induced shear bands in PETN with these calculations and found fair agreement between observed and calculated shear band spacing.

Several researchers have attempted to calculate the temperature rise in shear bands. Chaudrhi [33] calculated the maximum temperature rise expected for different plastic strain rates and concluded that high strain rates can create a temperature rise necessary to increase the temperature of HMX its above ignition temperature. He concluded that the maximum temperature is strongly dependent on the material melt temperature. Boyle, Frey and Blake [37] determined the maximum temperature rise in a shear band by imposing a shear velocity across an arbitrary thickness of several explosive samples. These researchers found that the maximum temperature in the shear band depended on pressure, shear velocity and material viscosity. They also derived an expression from their model which appeared to properly separate ignition and non-ignition occurring in

Table 2.1 Summary of Some Previous Viscoplastic Pore Collapse Models.

	melting treated?	Variable (Y, μ)	conduction treated in condensed-phase	gas in pore	chemical reactions	comments	results
Carroll [44]	no	constant Y, no viscosity considered	N.A.	no	N.A.	solved momentum eqn. with elastic-plastic work and kinetic energy: static loading	collapse in 3 phases, plastic phase most important, compressibility effects negligible
Butcher [14]	no	no	N.A.	no	N.A.	included deviatoric stress an viscous effects: dynamic loading	good agreement with experimental values for shock compression of porous Al
Khasainov [15]	no	no	no	no	no	low Re, pore diameter >> critical diameter at which conduction is negligible: viscoplastic heating: static loading : approximate solution of eqns.	Pore surface temperature is a linear function of time: ignition time estimated from this relationship
Khasainov [9]	no	no	yes	yes	no	low Re, viscous heating only, static loading, assumed tempurature profile in c-phase	for $a \gg a_{cr}$, Tmax is found, tign found by equating viscous work with energy required by thermal explosion theory
Dunin [16]	yes	no	no	no	no	low Re, viscoplastic heating	calculated critical Ps for melting to occur and extent of melt zone, determined that for $Ps > Ps_{cr}$ melting could cause total void closure
Attetkov [17]	yes	no	no	yes	no	low Re, non-dimensionalized equations, included viscpolastic effects	different collapse regimes for combinations of N.D. parameters, maximum heating possible for $a \gg a_{cr}$

8

Table 2.1 -- Continued

Frey [30]	yes	yes	yes	yes	no	numerical solution with viscoplastic heating and finite difference solution for conduction, pore pressurization rate, cavity size, material properties considered	viscoplastic work is dominant heating mechanism, favored by high μ, low Y, and high dP/dt, determined dP/dt parameter govering viscous/inertial collapse regime
Carroll [45]	yes	yes	no	yes	no	dynamic loading, viscoplastic effects, $a \gg a_{cr}$	initial temperature and property dependence on temperature is very important, inclusion of melting and temperature dependence can change colapse from viscous to inertial
Khalsinov [46]	yes	yes	yes	yes/ no	yes	considered two 1-step Arrhenius RXN mechanisms: c-phase (thermal explosion) with no pore gas and gas-phase: static loading and low Re	for thermal explosion model critical Ps required for given a, ϕ: gas phase model predicts ignition/quenching of reaction, critical Ps for sustained burning
Kang [7]	yes	yes	yes	yes	yes	detailed finite-rate kinetics, assumed Temperature distribution in c-phase for conduction, mass transfer to void, dynamic loading	predicted pore explosion due to reaction, material property effects, and porosity and pore size effects, examined pulse and ramp loading on ignition thresholds

experiments. Coffey [38] and Tamokoff, Fayer and Dlott [39] analyzed shear band generation by shock and impact and concluded that energy dissipation in the shear band is a quantum mechanical process called multiphonon up-pumping. In this mechanism, energy is transferred to molecule's internal vibrations by photons generated by shock induced dislocation movements.

In addition to those discussed above, descriptions of many other models appear in the literature [40-42]. Many of the models proposed to describe hot spot formation are of questionable value in predicting shock sensitivity of explosives. This is because most of the models mentioned above (with the exception of the gas compression model) do not relate parameters such as pressurization rate, porosity, pore size, and viscosity to ignition thresholds [30]. These parameters have been shown to be important in shock sensitivity of energetic materials.

2.3 Viscoplastic Hot Spot Models

One model that has success in predicting some of the above mentioned features, and is therefore popular among researchers, is the viscoplastic pore collapse model. (Some of these studies are summarized in Table 2.1). This model originated in the study of bubble collapse in liquids. Rayleigh [43] derived an ordinary differential equation describing the symmetrical collapse of a gas-filled bubble surrounded by an inviscid, incompressible liquid.

Experimental work by Zababakhin [15] has shown that the dynamics of bubble collapse in a viscous liquid depend strongly on a non-dimensional parameter that relates the viscous forces of collapse with the inertial forces. This parameter is referred to as the pore Reynolds number, and is defined as,

$$Re^* = a_0 \sqrt{\rho(p_s - p_{y0})} / \mu$$

(2.1)

where μ and ρ are the viscosity and density of the material surrounding the void, p_s is the shock pressure, p_{y0} is the plastic yield strength of the solid material and a_0 is the initial bubble diameter. For values of $Re^* > 8.4$, the bubble collapses very rapidly with inertial effects dominating. For this type of collapse the hydrodynamic collapse mechanism discussed above may be important [30]. For values of pore Reynolds number much less than 8.4, the collapse is viscous dominated, leading to much slower collapse velocities.

Carroll and Holt [44] developed a simplified hollow sphere model, similar to the bubble collapse model, to approximate the dynamic compaction behavior of shock-loaded porous materials. In this model, the inner sphere radius and porosity were assumed to be characteristic of the average void size and porosity of the material. A differential equation, which included the effects of elastic-plastic work and kinetic energy, was used to describe the spherically symmetric

10

collapse of the hollow sphere. Three phases of the pore collapse process were found; an initial elastic phase, a transitional elastic-plastic phase, and a plastic phase. The porosity change during the first two phases of collapse was found to be negligible. In addition, the effect of elastic compressibility on pore collapse was found to be small.

Butcher, Carroll, and Holt [14] improved the model by including deviatoric stress (porosity dependent yield strength) and material viscosity effects. They observed generally good agreement between experimentally obtained data for shock compaction in porous aluminum.

Khasainov, Borisov, and Ermolayev [15] modified the model to include the viscoplastic heating mechanism and calculated the critical pore radius needed to form hot spots for low pore Reynolds number collapse ($Re^* \ll 1$). By comparing the characteristic times for sphere cooling by conduction and viscous collapse, a critical pore diameter at which the influence of heat conduction becomes important was determined. This value was found to be,

$$a_0^* = 2\sqrt{\mu\alpha/(p_s - p_{yo})}$$

(2.2)

where α is the material thermal diffusivity. For pore sizes much greater than this critical value, conduction can be ignored, and most of the heat dissipated by viscoplastic work is localized very near the pore surface, leading to very high local temperatures. By neglecting conduction, an expression for the pore interface temperature as a linearly increasing function of time was derived. This expression was used to estimate the time required to the reach the ignition temperature of the explosive PETN.

By equating the energy generated by viscous heating with the chemical energy needed to produce thermal explosion of the material, Khasainov, Borisov, Ermolaev, and Korotov [36] derived an expression for ignition temperature. They then incorporated this model into a one-dimensional Lagrangian computer code to calculate hot spot growth to detonation in the explosive PETN.

Dunin and Surkov [16] and Attetkov, Vlasova, Selivanov, and Solov'ev [17] extended the model to include melting effects near the vicinity of the pore. Carroll, Kim, and Nesterenko [45] included melting effects and temperature-dependent material yield strength and viscosity. These researchers found that the inclusion of both melting and temperature dependent properties could result, under certain conditions, in the transition of the pore collapse from a viscous to an inertia dominated collapse, even for pore Reynolds number values less than one.

Frey [30] used this type of model to study the effects of pressurization rate, cavity size, and material properties on hot spot formation. He found that viscous heating is the most efficient heating mechanism and is dominant when the pressure rise time is short, viscosity is high, and/or

yield stress is low. In addition, the pressurization rate was found to have a large effect of the inertial / viscous collapse regime.

Each of these studies has shown that the viscoplastic heating mechanism is very efficient way to convert mechanical energy from pore collapse into heat, predicting high temperatures in the vicinity of the pore. Many of the temperatures predicted by these models are greater than experimentally observed temperatures required to initiate chemical decomposition of an energetic material. However, none of these models includes the affect of chemical decomposition of the energetic material.

Khasainov and others [46] extended the viscoplastic pore collapse model to include a single Arrhenius-type chemical reaction at the pore surface, mass transfer from the material to the pore gas, and a Arrhenius-type single gas-phase decomposition reaction. These researchers found that this model could describe both the initiation and quenching of a reactive hot spot, and used the model to predict the experimentally observed shock sensitivity on pore size and porosity.

In a more detailed viscoplastic hot spot model, Kang, Butler, and Baer [7] included detailed finite-rate chemical kinetics in the gas and condensed-phases, mass transfer from the condensed-phase to the gas-phase, heat conduction, melting, and variable material properties. They predicted the affect of material properties, pore size, and material porosity, on the ignition thresholds of an explosive subjected to constant and dynamic shock loading conditions.

3 MODEL FORMULATION

3.1 Introduction

The purpose of this section is to present a physical description and the governing conservation equations for viscoplastic hot spot formation in condensed-phase energetic materials. In Section 3.2, a brief description of the physical processes and the sequence of events believed to preceed viscoplastic hot spot formation is presented. A description of the geometrical configuration used in developing the mathematical model is presented in Section 3.3, and assumptions made to simplify the mathematical model are given in Section 3.4. In Section 3.5 the general form of the partial differential equations governing viscoplastic pore collapse are introduced. The interface, boundary, and initial conditions needed to solve the system of equations are also given in this section. To reduce the complexity of the system of PDE's and make an efficient numerical solution of the equations possible, the condensed-phase continuity and momentum equations along with the gas-phase equations are integrated to yield a set of ordinary differential equations (ODE's) for the motion of the pore interface, and for the macroscopic pore gas properties. This is outlined in Section 3.6.

3.2 Physical Description of Hot Spot Formation

Before proceeding with the mathematical analysis and development of a computational model to simulate viscoplastic pore collapse, it is instructive to first discuss some of the physical processes that occur during shock-induced void collapse in an energetic material. Previous research [7] suggests that hot spot formation by the viscoplastic mechanism may occur in a well-defined sequence of events. As a shock wave propagates through an energetic material, an increase in stress in the bulk of the material behind the shock wave occurs. For weak shock waves this stress is not enough to cause significant compression of the matrix material. However, the shock induced stress may be high enough to cause deformation of the material surrounding voids and other material irregularities [47]. It has been shown [44] that void collapse occurs in three distinct phases; i.) a totally elastic collapse phase, ii.) an elastic-plastic collapse phase, and iii.) a totally plastic collapse phase. Pore collapse in the elastic and elastic-plastic phases accounts for very little of the actual pore motion during collapse. Most of the pore motion takes place in the totally plastic collapse phase after yielding of the material has occurred.

During the final phase of collapse, mechanical energy is converted to thermal energy by viscous dissipation and local plastic work. The energy conversion leads to heating of the matrix material, and is dependent on the viscosity and plastic yield strength of the material. Viscoplastic heating is concentrated very near the surface of the void, in the region of the highest flow velocity (largest plastic deformation). As viscolastic heating of the matrix material occurs, heat is also

removed by conduction to the inert void gas and to the lower temperature matrix material. If heat removal by conduction is sufficient to balance heat generation by viscoplastic work, no temperature rise occurs in the material adjacent to the pore. However, if heat generation is greater than heat removal by conduction, the temperature near the pore surface increases, forming a thermal hot spot in the material.

At sufficiently high temperatures, melting and chemical decomposition of the condensed-phase material may occur. Decomposition at the void interface causes the transfer of chemically reactive vapors into the pore. Following an induction period when reactive vapors collect in the pore, the high gas pressures and temperatures, due to the compression of the gas during the collapse and heat transfer from the hot condensed-phase, may cause ignition of the reactive vapors. If the amount of heat released by the chemical reactions exceeds the heat conducted away from the pore, surface ignition of the gas-phase can transition to steady burning. On the contrary, the reaction quenches when energy losses due to thermal conduction exceed energy production from reaction.

3.3 Idealized Geometry for Hot Spot Model

In most cases of interest, voids present in energetic materials are of irregular shape. In the present study, however, an ideal hollow sphere geometry [44] is used to develop the mathematical description of hot spot formation by viscoplastic pore collapse. This geometry is shown in Fig. 3.1. Here, the inner pore radius is representative of the average pore size in a much larger sample of material containing multiple, randomly distributed voids. The porosity of the control volume is representative of the macroscopic material porosity, and is defined as;
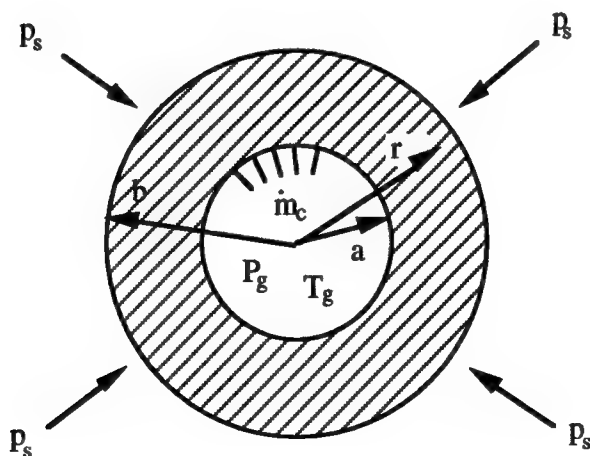

Fig. 3.1 Hollow-sphere geometry used to model viscoplastic hot spot formation.

14

$$\phi = \frac{V_g}{V_c + V_g} = \left(\frac{a}{b}\right)^3 \tag{3.1}$$

where V_g and V_c are the gas and condensed-phase volumes respectively, and a and b are the inner and outer pore radius of the hollow sphere.

3.4 Model Assumptions

In addition to assuming an idealized spherical geometry, several other assumption are made to reduce the complexity of the mathematical analysis. These assumptions, with justification, are:

1) The condensed-phase material is incompressible and isotropic. The assumption of incompressibility is valid for solids subjected to weak shock waves, since very strong shock waves are needed to produce compressibility effects in solids [47]. It has been shown [44] that most of the volume change that occurs during the compression of porous materials is due to the collapse of voids in the material.

2) The flow of the material is spherically symmetric in the vicinity of the void. This assumption is valid for cases where the time required for the shock wave to pass over the cavity is very short compared to the pore collapse time. For a 100 μm void, assuming a speed of sound of 2,500 meters per second (typical of solid energetic material), the shock transit time is approximately 40 ns. This is several orders of magnitude faster than the characteristic viscous collapse time.

3) The condensed-phase is an ideal, viscoplastic material. Figure 3.2 illustrates the stress-strain behavior of this type of material. Note that deformation occurs only in the totally plastic regime after the shock amplitude exceeds the material yield strength. This assumption is consistent with the observation of Carroll and Holt [44] that volume changes in the elastic and elastic-plastic phases of collapse are negligible.
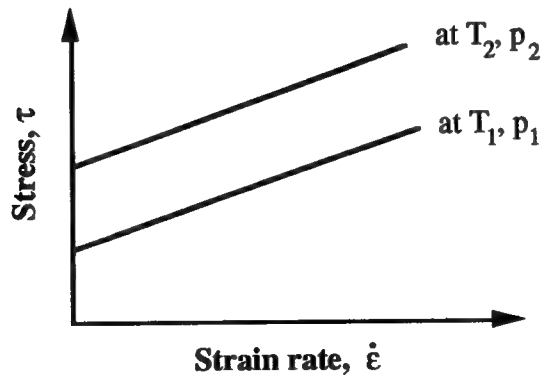

Fig. 3.2 Stress-strain rate curves for an ideal viscoplastic material.

4) Thermal conductivities of the gas and condensed-phases are constant. In addition, the specific heat of the condensed-phase is also assumed to be constant. It is very likely that these assumptions are not valid, due to the large temperature changes encountered during hot spot formation. However, the lack of experimental data for these quantities makes this assumption necessary.

5) Gas-phase pressure dependence is predicted by a real-gas equation of state. For the high density gas states possible during the pore collapse, the behavior of the gas phase is likely to deviate substantially from ideal gas behavior.

3.5 Governing Differential Equations in General Form

The mathematical model consists of a set of differential equations governing the transient processes occurring in the condensed and gas phases. The behavior of each of these regions is described by the continuity, momentum and energy equations. These governing equations along with the initial and boundary conditions for the model are described in the following sections.

3.5.1 General Form of the Condensed-Phase Governing Equations

For the one-dimensional, spherically symmetric flow of an incompressible, chemically reacting material, the Eulerian form of the governing conservation equations are written in general form below;

mass

$$\frac{\partial}{\partial r}\left(r^2 u_c\right) = 0 \tag{3.2}$$

momentum

$$\rho_c\left(\frac{\partial u_c}{\partial t} + u_c \frac{\partial u_c}{\partial r}\right) = \frac{\partial \sigma_r}{\partial r} + \frac{2}{r}\left(\sigma_r - \sigma_\theta\right) \tag{3.3}$$

energy

$$\rho_c c_c\left(\frac{\partial T_c}{\partial t} + u_c \frac{\partial T_c}{\partial r}\right) = \frac{1}{r^2}\frac{\partial}{\partial r}\left(k_c r^2 \frac{\partial T_c}{\partial r}\right) + \Phi_c - \sum_k \dot{\omega}_k h_k \tag{3.4}$$

species

$$\rho_c\left(\frac{\partial Y_k}{\partial t} + u_c \frac{\partial Y_k}{\partial r}\right) = \frac{1}{r^2}\frac{\partial}{\partial r}\left(\rho_c D_c r^2 \frac{\partial Y_k}{\partial r}\right) + \dot{\omega}_k \tag{3.5}$$

In the previous equations r and θ are the radial and tangential coordinates in the spherical coordinate system, and t represents time. For an ideal viscoplastic material the stresses appearing in the previous equations are defined as,

$$\sigma_r = -p_c - 4\mu_c \frac{u_c}{r} - \frac{2}{3}\overline{Y}_c \text{sign}(u_c)$$

(3.6)

$$\sigma_\theta = -p_c - 2\mu_c \frac{u_c}{r} - \frac{1}{3}\overline{Y}_c \text{sign}(u_c)$$

(3.7)

These stresses depend on the condensed-phase thermodynamic pressure, p_c, and the material properties viscosity, μ_c, and plastic yield strength, $\overline{Y}_c$. The $\text{sign}(u_c)$ convention is necessary to retain the proper directions of the stresses during pore collapse and subsequent expansion. For radial velocities greater than zero (pore expansion) the term $\text{sign}(u_c) = 1$. For pore collapse (negative velocities) $\text{sign}(uc) = -1$.

The energy conservation equation, (Eq. 3.4), is a balance between the internal energy accumulated at a radial position in the flow field, the energy convected away, the conduction of heat from the position, and the generation of heat by viscoplastic dissipation written as,

$$\Phi_c = 12\mu_c \frac{u_c^2}{r^2} + 2\overline{Y}_c \frac{|u_c|}{r}$$

(3.8)

A detailed description of the complete set of governing equations and derivations is given in [7].

3.5.2 General Form of the Gas-Phase Governing Equations

The gas-phase governing equations describing an unstaedy, compressible, chemically reacting flow are,

mass

$$\frac{\partial \rho_g}{\partial t} + \frac{1}{r^2}\frac{\partial}{\partial r}\left(\rho_g r^2 u_g\right) = 0$$

(3.9)

momentum

$$\rho_g\left(\frac{\partial u_g}{\partial t} + u_g \frac{\partial u_g}{\partial r}\right) = -\frac{\partial p_g}{\partial r} + \frac{1}{r^2}\frac{\partial}{\partial r}\left(r^2 \tau_{rr}\right) - \frac{2}{r}\tau_{\theta\theta}$$

(3.10)

17

energy

$$\rho_g c_{p,g}\left(\frac{\partial T_g}{\partial t}+u_g\frac{\partial T_g}{\partial r}\right)=\frac{1}{r^2}\frac{\partial}{\partial r}\left(k_g r^2\frac{\partial T_g}{\partial r}\right)+\rho_g D_g\sum_k\frac{\partial h_k}{\partial r}\frac{\partial Y_k}{\partial r}+\beta_g T_g\left(\frac{\partial p_g}{\partial t}+u_g\frac{\partial p_g}{\partial r}\right)$$

$$+\Phi_g-\sum_k\dot{\omega}_k h_k+\dot{q}_{rad} \tag{3.11}$$

species

$$\rho_g\left(\frac{\partial Y_k}{\partial t}+u_g\frac{\partial Y_k}{\partial r}\right)=\frac{1}{r^2}\frac{\partial}{\partial r}\left(\rho_g D_g r^2\frac{\partial Y_k}{\partial r}\right)+\dot{\omega}_k \tag{3.12}$$

equation of state

$$p_g=p_g(\rho_g,T_g) \tag{3.13}$$

Equation 3.9 expresses mass conservation for a spherically-symmetric volume of compressible, chemically reacting gas, where the quantities u_g and ρ_g represent the gas-phase velocity and density, respectively. The stress components in Eq. 3.10, which balances the inertial forces and the stresses occurring during gas compression, are written as,

$$\tau_{rr}=\frac{4}{3}\mu_g\left(\frac{\partial u_g}{\partial r}-\frac{u_g}{r}\right) \tag{3.14}$$

$$\tau_{\theta\theta}=-\frac{2}{3}\mu_g\left(\frac{\partial u_g}{\partial r}-\frac{u_g}{r}\right) \tag{3.15}$$

Equation 3.11, the gas-phase energy equation, contains many terms that are similar to those contained in the condensed-phase energy equation. These include the energy accumulation, convection, conduction, dissipation, expressed as,

$$\Phi_g=\frac{4}{3}\mu_g\left(\frac{\partial u_g}{\partial r}-\frac{u_g}{r}\right) \tag{3.16}$$

and chemical energy release term. In addition, the gas energy equation contains a compression work term, a term arising from the enthalpy flux carried by molecular species diffusion, and a radiation heat transfer term. Equation 3.12 is the species mass conservation expression for the gas

phase and Eq. 3.13 is an general expression of a real-gas equation of state that relates the gas pressure to gas density and temperature.

3.5.3 Interface, Boundary, and Initial Conditions

In order to solve the set of coupled, differential governing equations that comprise the mathematical model, the appropriate boundary and initial conditions must be specified. The initial conditions are:

$$u_c = u_g = 0 \tag{3.17a}$$

$$p_g = p_{go} \tag{3.17b}$$

$$T_c = T_g = T_o \tag{3.17c}$$

$$Y_k = Y_{ko} \tag{3.17d}$$

$$a = a_o \tag{3.17e}$$

$$b = b_o \tag{3.17f}$$

The boundary conditions at the inner pore radius, $r = a$, are;

$$\frac{\partial u_g}{\partial r} = 0 \tag{3.18a}$$

$$\frac{\partial T_g}{\partial r} = 0 \tag{3.18b}$$

$$\frac{\partial p_g}{\partial r} = 0 \tag{3.18c}$$

$$\frac{\partial Y_k}{\partial r} = 0 \tag{3.18d}$$

At the outer pore radius, $r = b$, the boundary conditions are,

$$\sigma_r = -p_s \tag{3.18e}$$

$$\frac{\partial T_c}{\partial r} = 0 \tag{3.18f}$$

19

In this research p_s is modeled as a sustained shock with a constant amplitude that is applied instantaneously at time, $t = 0$. At the boundary between the gas and condensed phases, mass, momentum, energy and species balances lead to the following equations;

mass

$$\left\{\rho_c(\dot{a} - u_c)\right\}_i = \left\{\rho_g(\dot{a} - u_g)\right\}_i = \dot{m}_c \tag{3.19a}$$

momentum

$$\left\{p_g - p_c - \frac{2\sigma}{a} - \tau_{rr,g} - \tau_{rr,c}\right\}_i = \left\{-\dot{m}_c u_c + \dot{m}_g u_g\right\}_i \tag{3.19b}$$

energy

$$\left\{\rho_g(e_g + \frac{1}{2}u_g^2)(u_g - \dot{a}) + \left[-k_g\frac{\partial T_g}{\partial r} + \rho_g\sum_k h_k(-D_g\frac{\partial Y_k}{\partial r})\right]\right.$$

$$-\rho_c(e_c + \frac{1}{2}u_c^2)(u_c - \dot{a}) + k_c\frac{\partial T_c}{\partial r} - \frac{2\sigma}{a}\dot{a}$$

$$\left.-u_g(-p_g + \tau_{rr,g}) + u_c(-p_c + \tau_{rr,c})\right\}_i = -\dot{q}_{i,rad} \tag{3.19c}$$

temperature

$$T_{c,i} = T_{g,i} \tag{3.19d}$$

species

$$\left\{\rho_c Y_k(u_c - \dot{a})\right\}_i - \left\{\rho_g Y_k(u_g - \frac{D_g}{Y_k}\frac{\partial Y_k}{\partial r} - \dot{a})\right\}_i = \dot{\omega}_{k,i} \tag{3.19e}$$

3.6 Reduced Form of the Governing Equations

The governing equations presented above form a general set of coupled PDE's that describe the dynamic and thermodynamic behavior of a hollow sphere subjected to an externally applied stress-time profile. It is possible to simplify many of these equations in order to make the numerical solution of the equations less computationally intensive. This section describes methods used to transform the condensed-phase mass and momentum equations and the gas-phase governing equations from PDE's to ODE's.

3.6.1 Motion of the Pore Interface

The integration of the condensed-phase mass and momentum equations, with the application of the proper interface and boundary conditions leads to an expression for the radial acceleration of the pore interface. The integration of the condensed-phase continuity equation (Eq. 3.2) with the substitution of the radial velocity interface condition (Eq. 3.19a) into the result, gives an expression for the velocity field in the condensed-phase. The resulting expression depends only on the radial position in the condensed phase and the position and velocity of the pore interface,

$$u_c = \frac{a^2}{r^2}\left(\dot{a} - \frac{\dot{m}_c}{\rho_c}\right)$$

(3.20)

where a is the pore radius, and $\dot{a}$ is the radial velocity of the pore radius.

By substituting the above expression for velocity (along its spatial and temporal derivatives), integrating from the inner radius, $r = a$, to the outer radius, $r = b$, and applying the momentum boundary conditions at these radii, an expression for the acceleration of the pore interface, $\ddot{a}$ is found,

$$\rho_c\left\{a\left(\ddot{a} - \frac{\ddot{m}_c}{\rho_c}\right)\left(1 - \phi^{1/3}\right) + \frac{1}{2}\left(\dot{a} - \frac{\dot{m}_c}{\rho_c}\right)\left[4\dot{a}\left(1 - \phi^{1/3}\right) - \left(\dot{a} - \frac{\dot{m}_c}{\rho_c}\right)\left(1 - \phi^{4/3}\right)\right]\right\}$$

$$= p_{g,i} - p_s - p_v + p_y - \dot{m}_c^2\left(\frac{1}{\rho_c} - \frac{1}{\rho_{g,i}}\right) - 2\frac{\sigma}{a}$$

(3.21)

where,

$$p_v = 12a^2\left(\dot{a} - \frac{\dot{m}_c}{\rho_c}\right)\int_a^b \frac{\mu_c}{r^4}dr$$

(3.22)

$$p_y = -2\mathrm{sign}(u_c)\int_a^b \frac{Y_c}{r}dr$$

(3.23)

The integral quantities, p_v and p_y represent the pressures arising from viscous and yield stresses that resist pore motion. By integrating the mass and momentum equations, the partial differential equation representing momentum conservation in the condensed phase is reduced to an ordinary differential equation for the acceleration of the pore interface. The solution of the pore motion acceleration equation for the velocity, and position of the pore interface allows the determination of the velocity field in the condensed-phase from Eq. 3.20.

21

3.6.2 Integrated Form of the Gas-Phase Equations:

The gas-phase governing equations (Eqs. 3.9 - 3.13) can also be reduced to ordinary differential equations by integrating the equations over the entire gas volume. The integral forms of the governing equations are then written in terms of the average gas properties in the pore. In order to simplify this analysis several other assumptions are made about the gas phase and gas-condensed phase interface;

1) The pressure is uniform throughout the gas phase. This assumption is valid for low Mach numbers in the gas phase.

2) The gas-phase normal viscous stress is small compared to the hydrostatic pressure at the pore interface, $(\tau_{rr})_{g,i} \ll p_{g,i}$.

3) The gas-phase conduction and diffusion heat flux can be expressed as [7],

$$\left\{ -k_g \frac{\partial T_g}{\partial r} + \rho_g \sum_k h_k(-D_g \frac{\partial Y_k}{\partial r}) \right\}_i = k_g \frac{T_g - T_{c,i}}{\delta_g} \tag{3.24}$$

where δ_g is the thermal boundary layer thickness in the gas phase.

4) The radiative heat flux is modeled as,

$$\dot{q}_{rad} = \varepsilon_g \sigma_{rad} \left(T_g^4 - T_{c,i}^4 \right) \tag{3.25}$$

The integrated gas-phase equations describing the average pore gas density, temperature, and species, are;

density

$$\frac{d\rho_g}{dt} = -\frac{3}{a} \left(\dot{a} - \frac{\dot{m}_c}{\rho_g} \right) \tag{3.26}$$

temperature

$$\rho_g c_{vg} \frac{dT_g}{dt} = \frac{3}{a} \left\{ k_g \frac{T_{c,i} - T_g}{\delta_g} + \varepsilon_g \sigma_{rad} (T_{c,i}^4 - T_g^4) - p_g \dot{a} \right.$$

$$\left. + \dot{m}_c (h_{g,i} + \frac{1}{2} u_{g,i}^2) - \sum_k e_{k,g} (\dot{\omega}_{k,i} + \dot{m}_c Y_{k,c}) \right\} - \sum_k (e_{k,g} \dot{\omega}_k) \tag{3.27}$$

22

species

$$\rho_g \frac{dY_k}{dt} = \dot{\omega}_k + \frac{3}{a}\left[\dot{\omega}_{k,i} + \dot{m}_c(Y_{k,c} - Y_k)\right]$$

(3.28)

equation of state

$$p_g = \frac{\rho_g R_g T_g}{1 - \eta \rho_g}$$

(3.29)

In Eq. 3.27, the integrated gas-phase energy equation, the rate of energy accumulation in the pore, is balanced by heat transfer to the condensed phase by conduction and radiation, work due to compression of the gas, and enthalpy flux into the pore due to mass transfer at the pore interface caused by chemical reaction. Energy is also generated by chemical reactions within the gas phase. Additionally, the interface energy condition can be simplified to;

$$k_{c,i}\frac{\partial T_c}{\partial r}\bigg|_{r=a} = -k_g \frac{(T_g - T_{c,i})}{\delta_g} + \varepsilon_g \sigma_{rad}(T_g^4 - T_{c,i}^4) +$$

$$\dot{m}_c\left[(h_{g,i} - h_{c,i}) + \frac{1}{2}(u_{g,i}^2 - u_{c,i}^2) + \frac{(\tau_{rr})_{c,i}}{\rho_c} - (u_{g,i} - u_{c,i})\dot{a}\right]$$

(3.30)

3.7 Approximation of the Condensed-Phase Energy Equation

In the previous section the reduced forms of the governing equations were presented. An integration technique was used to transform the general pore gas partial differential governing equations into ODE's describing the average pore gas temperature, density, and concentration. An ODE expression for the acceleration of the pore interface was derived from the integration of the condensed-phase mass and momentum equations. By writing the governing equations in ODE form it is possible to take advantage of efficient ODE numerical solution algorithms. The technique used to transform the condensed-phase energy equation from a PDE into an ODE is presented below.

Since the condensed-phase is deforming during pore collapse, it is convenient to use a Lagrangian form of the energy equation in the solution,

$$\rho_c c_c \frac{dT_c}{dt} = k_c\left(\frac{\partial^2 T_c}{\partial r^2} + \frac{2}{r}\frac{\partial T_c}{\partial r}\right) + \Phi_c + q_{ch}$$

(3.31)

23

where dT_c/dt represents the total time derivative of temperature for a particle mass that is convected with the flow. The contribution to the rate of temperature change for this particle involves viscous dissipation and plastic work, heat release by chemical reaction, and thermal conduction. Due to the thermal conduction term in the energy equation, the solution of this equation involves the determination of the temperature field in the condensed phase region. It is important to correctly model the condensed-phase thermal field, especially near the pore interface, since chemical decomposition and reaction in the condensed-phase is dependent on the material's temperature.

Rather than solve for the thermal field in the entire condensed-phase region, a previous approach in viscoplastic hot spot modeling [14,7] was to use a classical integral transformation method to develop an approximation to the interface temperature. This simplifies the problem by converting the energy PDE to a single ODE involving the interface temperature. However, the application of the classical integral approach requires the assumption of a thermal profile in the condensed-phase. Both exponential and polynomial expressions have been used for this purpose. Instead of introducing the assumption of a known temperature profile in the condensed-phase and using the classical integral approach to approximate the condensed-phase surface temperature, a finite difference method is used in the present model to solve the energy equation over the entire condensed-phase region. In the method of lines, the spatially dependent thermal conduction terms in the energy equation are replaced by algebraic approximations, which decouple the time and space variables. The result is a system of explicit ordinary differential equations in time results.

In order to derive finite-difference expressions to approximate the heat conduction term in the energy equation, the condensed-phase region must be discretized. Since the condensed phase is assumed to be incompressible, a Lagrangian grid system is convenient for this purpose. This grid is illustrated in Fig. 3.3, where the condensed-phase material is divided into n cells. From mass conservation considerations the location of each cell node can be determined from the location of the pore interface, a. The condensed-phase energy equation is solved at each cell node point, designated r_c in the figure.
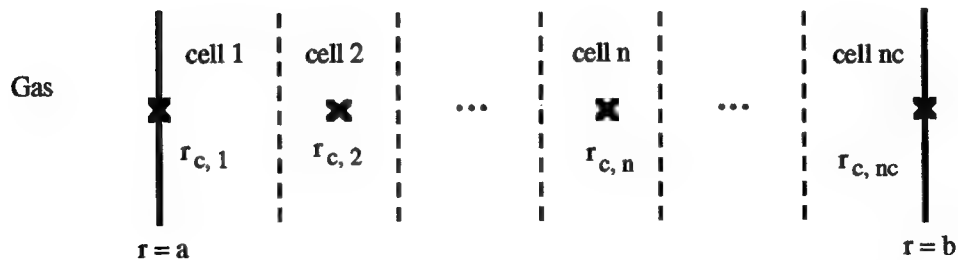

Fig. 3.4 Grid used to derive finite-difference approximations to the conduction term in the condensed-phase energy equation.

24

In this model, Taylor series expansions are used to derive general, second order, finite-difference approximations for the spatial derivatives in the condensed-phase energy equation.

At any interior grid point $(2 < n < nc-1)$ the first derivative is approximated by the expression,

$$\frac{\partial T_{c,n}}{\partial r} \approx \left\{ \frac{1}{(r_{c,n+1} - r_{c,n-1})} \right\} \cdot \left\{ \frac{(r_{c,n} - r_{c,n-1})(T_{c,n+1} - T_{c,n})}{(r_{c,n+1} - r_{c,n})} \right. $$

$$\left. - \frac{(r_{c,n+1} - r_{c,n})(T_{c,n-1} - T_{c,n})}{(r_{c,n} - r_{c,n-1})} \right\} \tag{3.32}$$

The explicit radial grid point distances, $(r_{c,n+1} - r_{c,n})$, $(r_{c,n} - r_{c,n-1})$, and $(r_{c,n+1} - r_{c,n-1})$ are retained in the finite-difference approximation due to deformation of the grid during pore collapse. Equation 3.32 reduces to the familiar second-order, central difference approximation,

$$\frac{\partial T_{c,n}}{\partial r} \approx \frac{T_{c,n+1} - T_{c,n-1}}{2\Delta r}$$

if the radial distances between the cell control points are uniform.

The first derivative at the inner boundary node, $n = 1$, is specified by Eq. 3.30, the interface energy equation,

$$\frac{\partial T_{c,1}}{\partial r} = -\frac{1}{k_c} \left\{ -k_g \frac{(T_g - T_{c,1})}{\delta_g} + \varepsilon_g \sigma_{rad}(T_g^4 - T_{c,1}^4) + \dot{m}_c(h_{g,i} - h_{c,i}) \right\} \tag{3.33}$$

where the interface temperature $T_{c,i}$ in Eq. 3.30 is replaced by $T_{c,1}$, and the kinetic energy terms due to mass flux at the interface are assumed to be small compared to chemical heat release and are therefore neglected.

At the outer boundary $(r = b,$ corresponding to node nc), the first derivative from Eq. 3.18f, is,

$$\frac{\partial T_{c,nc}}{\partial r} = 0 \tag{3.34}$$

Taylor series expansions are also used to derive the approximations of the second derivatives. At an interior grid point, $2 < n < nc-1$, the second-order finite difference is

$$\frac{\partial^2 T_{c,n}}{\partial r^2} \approx \left\{ \frac{2}{(r_{c,n+1} - r_{c,n-1})} \right\} \left\{ \frac{(T_{c,n+1} - T_{c,n})}{(r_{c,n+1} - r_{c,n})} + \frac{(T_{c,n-1} - T_{c,n})}{(r_{c,n} - r_{c,n-1})} \right\} \tag{3.35}$$

where this expression reduces to the uniform-grid, second order, central finite difference for the second derivative,

$$\frac{\partial^2 T_{c,n}}{\partial r^2} \approx \frac{T_{c,n+1} - 2T_{c,n} + T_{c,n-1}}{\Delta r^2}$$

A Taylor series expansion which incorporates the boundary condition at the inner pore radius is used to derive the approximation for the second derivative at node n = 1. The derivative approximation is;

$$\frac{\partial^2 T_{c,1}}{\partial r^2} \approx \left\{ \frac{2}{\Delta r_2 - \Delta r_3} \right\} \left\{ \frac{\Delta r_2}{\Delta r_3^2} (T_{c,3} - T_{c,2}) - \frac{\Delta r_3}{\Delta r_2^2} (T_{c,2} - T_{c,1}) \right\}$$

$$-2 \left\{ \frac{\Delta r_2 + \Delta r_3}{\Delta r_2 \Delta r_3} \right\} \frac{dT_{c,1}}{dr} \tag{3.36}$$

where, $\Delta_r^2 = (r_{c,2} - r_{c,1})$ and $\Delta_r^3 = (r_{c,3} - r_{c,1})$. By substituting the finite-difference approximations to the conduction term into Eq. 3.31, the condensed-phase energy equation at grid point n becomes,

$$\rho_c c_c \frac{dT_{c,n}}{dt} = k_c \left(T_{c,n}'' + \frac{2}{r_{c,n}} T_{c,n}' \right) + \Phi_{c,n} + q_{ch,n} \tag{3.37}$$

where T_{cn}' and T_{cn}'' represent the first and second derivative finite-difference approximations, respectively, $\Phi_{c,n}$ is the energy dissipation term, and $q_{ch,n}$ is the chemical energy generation term at node n. The solution of the condensed-phase energy equation over the entire condensed-phase domain gives rise to a total of nc ordinary differential equations for the condensed-phase thermal field.

Table 3.1 Variables in the Condensed-Phase Governing Equations

variable	description	units
ρ_c	condensed-phase density	g / cm^3
c_c	specific heat	ergs / (g-K)
k_c	thermal conductivity	ergs / (cm-s-K)
μ_c	viscosity	g / (cm-s)
Y_c	plastic yield strength	dyne / cm^2
p_c	pressure at radial position in condensed phase	dyne / cm^2
u_c	condensed-phase radial velocity	cm / s
σ_r	condensed-phase principal radial stress	dyne / cm^2
σ_θ	condensed-phase principal tangential stress	dyne / cm^2
T_c	condensed-phase temperature	K
Φ_c	viscoplastic energy dissipation term	ergs / (cm^3 - s)
Y_k	condensed-phase species k	non-dimensional
$\dot{\omega}_k$	rate of production of species k by chemical reactions	g / (cm^3 - s)

Table 3.2 Variables in the Gas-Phase Governing Equations

variable	description	units
ρ_g	density	g / cm^3
c_{p_g}	specific heat at constant pressure	$ergs / (g\text{-}K)$
k_g	thermal conductivity	$ergs / (cm\text{-}s\text{-}K)$
μ_g	viscosity	$g / (cm\text{-}s)$
D_g	mass diffusivity	cm^2 / s
p_g	gas pressure	$dyne / cm^2$
u_g	gas-phase radial velocity	cm / s
τ_{rr}	gas-phase principal radial stress	$dyne / cm^2$
$\tau_{\theta\theta}$	gas-phase principal tangential stress	$dyne / cm^2$
T_g	gas-phase temperature	K
h_k	specific enthalpy of species k	$ergs / g$
Φ_g	dissipation	$ergs / (cm^3\text{-}s)$
$\dot{\omega}_k$	production rate of species k	$g / (cm^3\text{-}s)$
β_g	gas-phase isobaric expansion coefficient	$1 / K$

4 RESULTS AND DISCUSSION

4.1 Introduction

It has been shown previously that viscoplastic heating is an effective mechanism in producing localized, high temperature regions capable of causing chemical decomposition in energetic materials. Hot spot formation due to viscoplastic pore collapse is a complex phenomenon that depends on many different processes. These include viscous and plastic heating, heat conduction, melting, and chemical reactions. In order to isolate some of the salient features involved in viscoplastic hot spot formation, namely the affects of viscous and plastic heating, and conduction, this section presents some results obtained from model simulations conducted for a material that is not allowed to undergo chemical decomposition. Section 4.2 presents some of the important model variables for a simplified case of pore collapse in the explosive RDX which is not allowed to undergo chemical reaction. The affects of material parameters such as initial pore radius on hot spot formation are shown here.

4.2 Constant Property Model

When a shock wave is applied to the hollow sphere shown in Fig. 3.1, the response of the material surrounding the void is determined by several factors including the shock pressure, the yield strength and viscosity, and the void size. The following results show some of the characteristics of the dynamics of the pore collapse process when the condensed-phase material properties, yield strength and viscosity are held constant. Initial conditions used in this case are summarized in Table 4.1.

Figures 4.1 through 4.4 show the temporal variation of some of the key thermophysical properties predicted by the model during pore collapse. Results for three different shock pressures are illustrated (250, 500, and 1000 MPa). The shock pressures studied here are an order of magnitude below the level required to shock initiate the virgin material (i.e., no voids). However, as demonstrated by Baillou, it is possible at these shock pressures to initiate reaction in a sample containing defects (micron-sized voids). Figure 4.1 shows that the pore collapses smoothly to an equilibrium value, with the final radius and the collapse rate determined by the shock magnitude. As the pore collapses, it is known that heat is generated in the condensed-phase material due to viscous dissipation and plastic work. The viscoplastic heating effects are localized near the surface of the void. The right-hand axis of Figs. 4.2a through 4.2c show the increase in pore interface temperature during collapse for each of the three shock pressures studied. The left-hand axis indicates the magnitude of each term in the condensed-phase energy equation (3.19c) when evaluated at the interface, $r = a$. The rate of temperature increase at the interface depends on the collapse velocity, and therefore the high shock pressures give rise to

Table 4.1 Initial Conditions and Constant Values

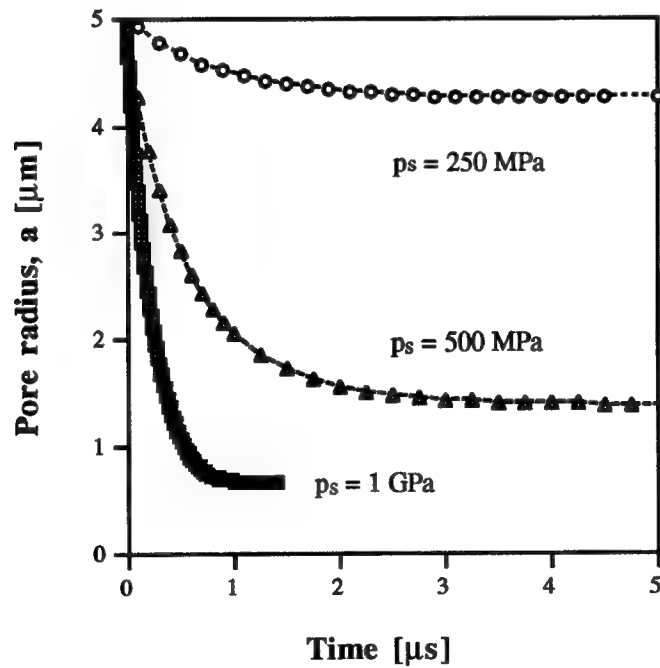| Variable	Value	Units
a_o	5.0×10^{-6}	m
$\dot{a}_o$	0.0	m / s
ϕ_o	0.05	none
$T_{co} = T_{go} = T_o$	300.0	K
P_{go}	1×10^5	Pa
m_{co}	50.0	m^2 / s
Y_{co}	1.1×10^8	Pa
ρc	1806.0	kg / m^3
k_c	0.260	W / (m-K)
k_g	0.083	W / (m-K)
c_c	1760.0	J / (kg-K)
c_{pg}	1000.0	J / (kg-K)
σ_g	5.67×10^{-8}	$W / (cm^2\text{-}K^4)$
η	1.0	m^3/kg

Fig. 4.1 Temporal variation of pore radius for three shock pressures.

30

higher heating rates and higher maximum interface temperatures. This feature is illustrated in these figures. When the pore collapse terminates, thermal conduction effects become dominant (since deformation of the material no longer occurs), and the heat at the interface is conducted radially to the condensed-phase material surrounding the void. The time at which this cross-over occurs (i.e., the dominant term of the energy equation) corresponds to the time at which minimum pore radius is reached. For example, for the case of p_s = 250 MPa, it occurs at approximately t = 2 μs, whereas for p_s = 1 GPa, it occurs much sooner (t = 0.75 μs). The point of cross-over also corresponds to a decrease in temperature from the peak values.

Pore gas pressure variation with time is shown in Figs. 4.3 for the three shock pressures considered. Heating of the gas by compression leads to very high gas temperatures and pressures for the high shock strength case (1 GPa). Since the pore collapses until the resistive stresses in the condensed-phase material and pore gas pressure balance the external shock pressure, rapid gas pressurization can be an important consideration in hot spot formation.
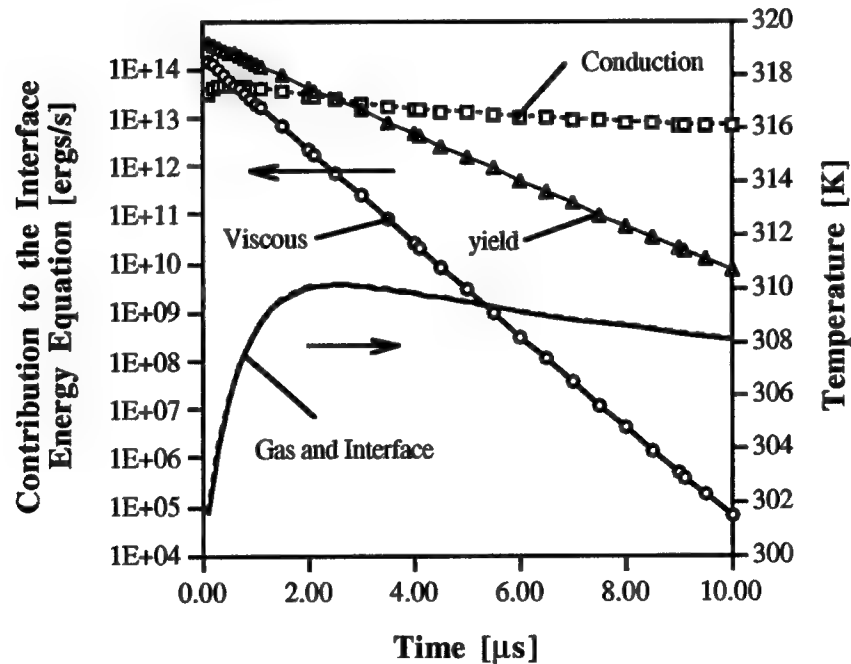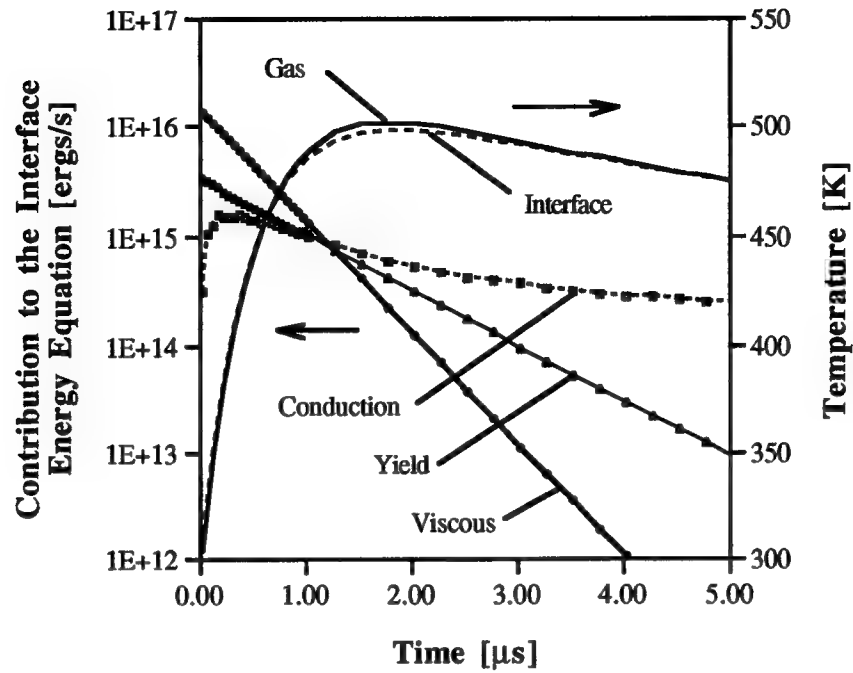

Fig. 4.2a Temporal variation of the pore interface and gas temperatures and the contribution of the three components in the condensed-phase energy equation. The applied shock pressure is P_s = 0.25 MPa.

31

Fig. 4.2b Temporal variation of the pore interface and gas temperatures and the contribution of the three components in the condensed-phase energy equation. The applied shock pressure is $P_s = 0.5$ GPa.
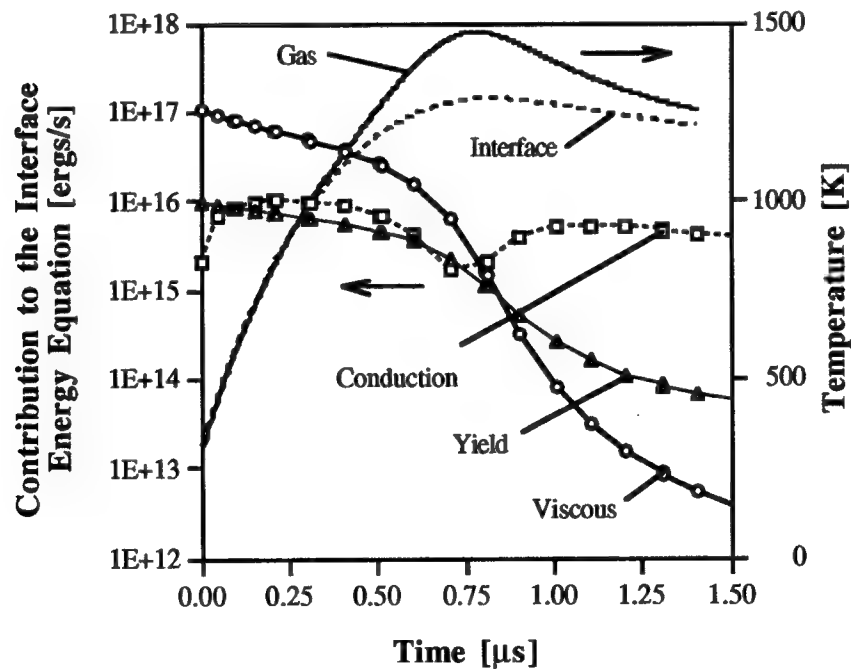

Fig. 4.2c Temporal variation of the pore interface and gas temperatures and the contribution of the three components in the condensed-phase energy equation. The applied shock pressure is $P_s = 1$ GPa.
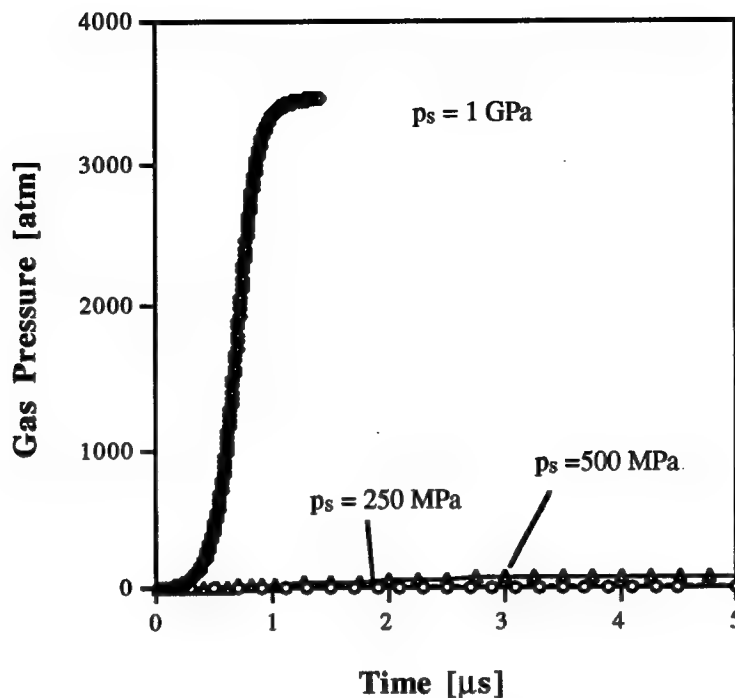
Figure 4.3 Temporal variation of the pore gas pressure for three shock pressures.

4.3 Summary

From the results presented here, it is evident that viscoplastic heating can be an effective mechanism for hot spot formation. However, it seems unrealistic to expect temperatures on the order of several thousand degrees in the condensed-phase material as predicted here. At such high temperatures it is expected that the condensed-phase material will melt. Melting requires latent heat removal which will affect heating. In addition, at high temperatures near the melting point, the yield strength, and viscosity of the material will likely decrease, with the yield strength going to zero as the material liquefies and can no longer resist stresses. For this reason it is important in future models to include melting and temperature and pressure dependent properties in the model. It is generally accepted that melting and the variation of the condensed-phase viscosity and yield strength will have an affect on hot spot formation in energetic materials.

REFERENCES

1. Boggs, T.L., "The Thermal Behavior of RDX and HMX," Progress in Astronautics and Aeronautics: Fundamentals of Solid-Propellant Combustion, Vol. 90, 1984, pp.121-175.

2. Mellor, A.M., Mann, D.M., Boggs, T.L., Dickinson, C.W., and Roe, W.E., "Hazard Initiation in Energetic Materials: Status of Technology Assessment," Combustion Science and Technology, Vol. 54, 1987, pp. 203-215.

3. Sutton, G.P., Rocket Propulsion Elements, 6th ed., John Wiley and Sons, 1992.

4. Mellor, A.M., Boggs, T.L., Covino, J., Dickinson, C.W., Dreitzler, D., Thorn, L.B., Frey, R.B., Gibson, P.W., Roe, W.E., Kirshenbaum, M., and Mann, D.M., "Research Needs and Plan for Energetic Material Hazard Mitigation," Combustion Science and Technology, Vol. 59, 1988, pp. 391-400.

5. Coffey, C.S., DeVost, V.F., and Woody, D.L., "Towards Developing the Capability to Predict the Hazard Response of Energetic Materials Subjected to Impact," Preprints of 9th Symposium (International) on Detonation, Portland, OR., 1989, pp. 965-974.

6. Setchell, R.E., and Taylor, P.A., "The Effects of Grain Size on Shock Initiation Mechanisms in Hexanitrostilbene (HNS) Explosive," Progress in Astronautics and Aeronautics: Dynamics of Shock Waves, Explosions and Detonations, Vol. 94, 1984, pp.350-368.

7. Kang, J., Butler, P.B., and Baer, M.R., "A Thermomechanical Analysis of Hot Spot Formation in Condensed-Phase, Energetic Materials," Combustion and Flame, Vol. 89, 1992, pp. 117-139.

8. Baillou, F., Dartyge, J.M., Spyckerelle, M., and Mala, J., "Influence of Crystal Defects on Sensitivity of Explosives," 10th Symposium (International) on Detonation, Boston, 1993.

9. Khasainov, B.A., Borisov, A.A., Ermolaev, B.S., and Korotkov, A.I., "Two-phase visco-plastic model of shock initiation of detonation in high density pressed explosives," 7th Symposium (International) on Detonation, Annapolis, MD, 1981.

10. Frey, R.B., "The initiation of explosive charges by rapid shear," 7th Symposium (International) on Detonation, Annapolis, MD, 1981.

11. Taylor, P.A., "The Effects of material microstructure on the shock sensitivity of porous granular explosives," 8th Symposium (International) on Detonation, Albuquerque, NM, 1985.

12. Coffey, C.S., "Hot spot production by moving dislocations in a rapidly deforming crystalline explosive," 8th Symposium (International) on Detonation, Albuquerque, NM, 1985.

13. Kim, K., and Sohn, C.H., "Modeling of reaction buildup processes in shocked porous explosives," 8th Symposium (International) on Detonation, Albuquerque, NM, 1985.

14. Butcher, B.M., Carroll, M.M., and Holt, A.C., "Shock-wave Compaction of Porous Aluminum," Journal of Applied Physics, Vol. 45, 1974, pp.3864-3875.

15. Khasainov, B.A., Borisov, A.A., and Ermolayev, B.S., "Shock Wave Predetonation Processes in Porous High Explosives," Progress in Astronautics and Aeronautics: Shock Waves, Explosions, and Detonations, Vol. 87, 1983, pp. 492-504.

16. Dunin, S.Z., and Surkov, V.V., "Effects of Energy Dissipation and Melting on Shock Compression of Porous Bodies", Journal of Applied Mechanics and Technical Physics, Vol. 23, 1982, pp.123-134

17. Attetkov, A.V., Vlasova, L.N., Selivanov, V.V., and Solov'ev, V.S., "Local Heating of a Material in the Vicinity of a Pore upon its Collapse", Journal of Applied Mechanics and Technical Physics, Vol. 25, 1984, pp.286-291.

18. Maiden, D.E., "A Model for Calculating the Threshold for Shock Initiation of Pyrotechnics and Explosives," Proceedings of the 12th International Pyrotechnics Seminar, Vail, CO, 1986, pp. 813-826.

19. Eyring, H., Powell, R.E., Duffey, G.H., and Parlin, R.B., "The Stability of Detonations," Chemical Reviews, Vol. 45, 1949, pp. 69-181.

20. Fauquignon, C., "The Two-Step Reaction Zone Structure: A Way to Interpret Non-Ideal Detonation Observations," ISL Report.

21. Field, J.E., "Hot Spot Ignition Mechanisms for Explosives," Accounts of Chemical Research, Vol. 25, 1992, pp. 489-496.

22. Field, J.E., Bourne, N.K., Palmer, S.J.P., and Walley, S.M., "Hot-Spot Ignition Mechanisms for Explosives and Propellant," Philosophical Transactions of the Royal Society of London: Series A, Vol. 339, 1992, pp. 269-283.

23. Krishna Mohan, K., Field, J.E., and Swallowe, G.M., "Effects of Physiacl Inhomogeneities on the Impact Sensitivity of Solid Explosives: A High-Speed Photographic Study," Combustion Science and Technology, Vol. 40, 1984, pp. 269-278.

24. Bowden, F.P., and Yoffee, A.D., Initiation and Growth of Explosion in Liquids and Solids, Cambridge University Press, 1952.

25. Chaudhri, M.M., and Field, J.E., "The Role of Rapidly Compressed Gas Pockets in the Initiation of Condensed Explosives," Proceedings of the Royal Society of London, Vol. A340, 1974, pp. 113-128.

26. Field, J.E., Swallowe, G.M., and Heavens, S.N., "Ignition Mechanisms of Explosives during Mechanical Deformation," Proceedings of the Royal Society of London, Vol. A382, 1982, pp. 231-244.

27. Starkenburg, J., "Ignition of Solid High Explosive by Rapid Compression of an Adjacent Gas Layer," 7th Symposium (International) on Detonation, Annapolis, MD, 1981, pp. 3-16.

28. Bourne, N.K., and Field, J.E., "Shock-Induced Collapse of Single Cavities in Liquids," Journal of Fluid Mechanics, Vol. 244, 1992, pp. 225-240.

29. Partom, Y., "A Void Collapse Model for Shock Initiation," 7th Symposium (International) on Detonation, Annapolis, MD, 1981, pp. 506-516.

30. Frey, R.B., "Cavity Collapse in Energetic Materials," 8th Symposium (International) on Detonation, Albuquerque, NM, 1985, pp. 68-80.

31. Mader, C.L., "Initiation of Detonation by the Interaction of Shocks with Density Discontinuities," The Physics of Fluids, Vol. 8, 1965, pp. 1811-1816.

32. Mader, C.L., Numerical Modelling of Detonations, Los Alamos Series in Basic and Applied Science, University of California Press, 1979.

33. Chaudhri, M.M., "The Initiation of Fast Decomposition in Solid Explosives by Fracture, Plastic Flow, Friction, and Collapsing Voids," Preprints of 9th Symposium (International) on Detonation, Portland, OR, 1989, pp. 331-339.

34. Field, J.E., Parry, M.A., Palmer, S.J.P., and Huntley, J.M., "Deformation and Explosive Properties of HMX Powders and Polymer Explosives," Preprints of 9th Symposium (International) on Detonation, Portland, OR, 1989, pp. 771-780.

35. Grady, D.E., and Kipp, M.E., "The Growth of Unstable Thermoplastic Shear with Application to Steady-wave Shock Compression in Solids," Journal of Mechanics and Physics of Solids, Vol. 35, 1987, pp.95-

36. Krishna Mohan, V., Jyothi Bhasu, V.C., and Field, J.E., "Role of Adiabatic Shear Bands in Initiation of Explosives by Drop Weight Impact," Preprints of 9th Symposium (International) on Detonation, Portland, OR, 1989, pp. 557-564.

37. Boyle, V., Frey, R., and Blake, O., "Combined Pressure Shear Ignition of Explosives," Preprints of 9th Symposium (International) on Detonation, Portland, OR, 1989, pp. 1-11.

38. Coffey, C.S., "Initiation of Explosive Crystals by Shock or Impact," Preprints of 9th Symposium (International) on Detonation, Portland, OR, 1989, pp. 864-870.

39. Tokmakoff, A., Fayer, M.D., and Dlott, D.D., "Chemical Reaction Initiation and Hot-Spot Formation in Shocked Energetic Materials," Journal of Physical Chemistry, Vol. 97, 1993, pp.1901-1913.

40. Lee, E.L., and Tarver, C.M., "Phenomological Model of Shock Initiation in Heterogeneous Explosives," Physics of Fluids, Vol. 23, 1980, pp.2362-2372.

41. Tang, P., "A Study of Detonation Processes in Heterogeneous High Explosives," Journal of Applied Physics, Vol. 63, 1988, pp.1041-1045.

42. Tang, P.K., Johnson, J.N., and Forest, C.A., "Modeling Heterogeneous High Explosive Burn with an Explicit Hot Spot Process," 8th Symposium (International) on Detonation, Albuquerque, NM, 1985, pp. 52-61.

43. Rayleigh, L., "On the pressure developed in a liquid during the collapse of a spherical cavity," Phil. Mag., Vol. 34, 1917, pp. 94-98.

44. Carroll, M.M., and Holt, A.C., "Static and Dynamic Pore-Collapse Relations for Ductile Porous Materials," Journal of Applied Physics, Vol. 43, 1972, pp. 1626-1635.

45. Carroll, M.M., Kim, K.T., and Nesterenko, V.F., "The Effect of Temperature on Viscoplastic Pore Collapse," Journal of Applied Physics, Vol. 59, 1986, pp.1962-1967.

46. Khasainov, B.A., Attetkov, A.V., Borisov, A.A., Ermolayev, B.S., Soloviev, V.S., "Critical Conditions for Hot Spot Evolution in Porous Explosives," <u>Progress in Astronautics and Aeronautics: Dynamics of Explosions</u>, Vol. 114, 1988, pp. 303-321.

47. Graham, R.A., <u>Solids Under High-Pressure Shock Compression</u>, Springer-Verlag, 1993.